

**Under-ice acoustic navigation using real-time model-aided range estimation**

EeShan C. Bhatt,<sup>1, 2, a</sup> Oscar Viquez,<sup>2</sup> and Henrik Schmidt<sup>2</sup>

<sup>1</sup>*MIT-WHOI Joint Program in Oceanography/Applied Ocean Science & Engineering,  
Cambridge and Woods Hole, MA, USA*

<sup>2</sup>*Department of Mechanical Engineering, Massachusetts Institute of Technology,  
Cambridge, MA*

(Dated: 20 February 2022)

1 The long baseline (LBL) underwater navigation paradigm relies on the conversion  
2 of recorded travel times into pseudoranges to trilaterate position. For real-time op-  
3 erations, this conversion has assumed an isovelocity sound speed. For re-navigation  
4 in post-processing, computationally and/or labor intensive acoustic modeling may  
5 be employed to reduce uncertainty driven by multipath arrivals. This work demon-  
6 strates a real-time ray-based prediction method of the effective sound speed along  
7 a path from source to receiver to minimize vehicle position error. This method was  
8 implemented for a small scale AUV-LBL system in March 2020, in the Beaufort Sea,  
9 in total ice-covered conditions and a double ducted acoustic propagation environ-  
10 ment. The vehicle was successfully deployed and recovered. Given the lack of GPS  
11 data throughout the vehicle’s mission, however, the pseudorange performance is first  
12 evaluated on connections between GPS-linked beacons. The real-time ranging error  
13 between beacons is roughly 11 meters at distances up to 3 km. But a consistent over-  
14 estimation in the real-time method provides insights for improved eigenray filtering  
15 by the number of surface bounces. An operationally equivalent pipeline is used to  
16 re-position the LBL beacons and re-navigate the AUV, using a modeled, historical,  
17 and a locally observed sound speed profile. The median re-navigation error is  $1.84 \pm 2.19$  RMS m. The improved trilateration performance for suggests that this ap-  
18 proach effectively extends the single meter accuracy of the deployed GNSS units into  
19 the water column.

---

<sup>a</sup>[ebhatt@whoi.edu](mailto:ebhatt@whoi.edu)

<sup>21</sup> **I. INTRODUCTION**

<sup>22</sup> Autonomous underwater vehicles (AUVs) are increasingly capable platforms to explore  
<sup>23</sup> and sample the ocean, particularly for remote and/or dangerous regions. However, navi-  
<sup>24</sup> gation uncertainty is a major challenge in considering AUVs as standard tools for oceano-  
<sup>25</sup> graphic research. While land and air-based robots utilize information from Global Naviga-  
<sup>26</sup> tion Satellite Systems (GNSS) to achieve stunning location accuracy and precision through-  
<sup>27</sup> out the duration of their missions, AUVs cannot access GNSS fixes while underwater. There-  
<sup>28</sup> fore, underwater vehicles have relied on any combination of dead reckoning, hydrodynamic  
<sup>29</sup> models, inertial navigation systems, doppler velocity logs, and acoustic baseline positioning  
<sup>30</sup> systems for navigation (Paull *et al.*, 2014). Limiting navigation error and drift requires an  
<sup>31</sup> AUV to periodically stall on the surface and obtain a GNSS fix to reset its position error.  
<sup>32</sup> This foolproof method of self-positioning is undesirable for stealth, adverse weather condi-  
<sup>33</sup> tions, and mission efficiency, and inaccessible in a GNSS-denied situation like an ice-covered  
<sup>34</sup> environment.

<sup>35</sup> Of underwater acoustic navigation systems, long baseline (LBL) is the most GPS-like  
<sup>36</sup> in style and scale, and most appropriate for mitigating drift without overburdening com-  
<sup>37</sup> putation or payload size on the vehicle (Van Uffelen, 2021). The state-of-the-art for LBL  
<sup>38</sup> outsources depth to a pressure sensor and solves the two-dimensional localization problem  
<sup>39</sup> with an isovelocity, linear scaling between one way travel time (OWTT) and range (Eustice  
<sup>40</sup> *et al.*, 2006, 2007; Webster *et al.*, 2009, 2012). This assumption is valid for short scale  
<sup>41</sup> operations but oversimplifies propagation for larger and/or complex acoustic environments.

42 To achieve single meter, GNSS-like performance in a GNSS-denied environment, we demon-  
 43 strate an embedded ray-based data processing algorithm to convert recorded OWTTs into  
 44 pseudorange estimates. This methodology was integrated onto the AUV *Macrura*, deployed  
 45 and recovered in the Beaufort Sea, in March 2020, during the Ice Exercise 2020 (ICEX20).  
 46 A physics-driven methodology that received an *in situ* sound speed profile (SSP) was nec-  
 47 essary despite the small operational domain because of the relatively high-risk mission en-  
 48 vironment—total under-ice conditions and a variable double ducted acoustic environment.  
 49 For consistency, we delineate specific definitions for timing, positioning, and navigation  
 50 from [Howe et al. \(2019\)](#).

- 51     1. Timing is the ability to acquire and maintain accurate and precise time anywhere in  
 52         the domain of interest within user-defined timeliness parameters
- 53     2. Positioning is the ability to accurately and precisely determine one's location refer-  
 54         enced to a standard geodetic system
- 55     3. Navigation is the ability to determine current and desired position (relative or absolute)  
 56         and apply corrections to course, orientation, and speed to attain a desired position  
 57         anywhere in the domain of concern

58 Thus, navigation is inherently in real-time and depends on positioning; positioning depends  
 59 on timing. We also suggest re-navigation and re-positioning as post-processed corollaries,  
 60 which may include knowledge or processing capabilities not available *in situ*.

61     While RAFOS floats championed one way ranging for re-positioning ([Duda et al., 2006](#);  
 62 [Rossby et al., 1986](#)), the ability to do so for navigation was facilitated by the advent of

the WHOI Micro-Modem (Singh *et al.*, 2006) and synchronized clocks (Rypkema *et al.*, 2017). AUV navigation efforts have achieved root mean square (RMS) localization error on the order of tens of meters relative to GNSS surface position over less than ten kilometers in shallow (Claus *et al.*, 2018; Eustice *et al.*, 2007; Kepper *et al.*, 2017) and deep water (Jakuba *et al.*, 2008; Kunz *et al.*, 2008; Webster *et al.*, 2009). However, these efforts all used a nominal sound speed for travel time conversion and the vehicles were limited to shallower isovelocity regimes.

Localization algorithms that do consider environmental or acoustic uncertainty tend to focus on longer and larger experiments, where spatio-temporal variability cannot be ignored. These methods have also been reserved for post-processing as they can be labor intensive, computationally heavy, and/or require additional information like contemporaneous data. For example, gliders navigating with kinematic flight models and equipped with acoustic modems were later unambiguously associated with predicted ray arrivals, resulting in roughly a kilometer error and hundred meters uncertainty over basin scale propagation (Van Uffelen *et al.*, 2013). A follow up study investigated how a single temporally and spatially averaged SSP could mitigate position error for a four month glider mission (Uffelen *et al.*, 2016). Wu *et al.* (2019) cross correlate three days of real acoustic records with synthetic ones generated through ocean model snapshots from HYCOM (Chassagnet *et al.*, 2007). While potentially applicable for various ocean states, this is reliant on model realism and impractical for real-time operations. Mikhalevsky *et al.* (2020) introduces a “cold start” algorithm that does not require prior knowledge of track, position, or sound speed information. The algorithm inputs a four-dimensional ocean model, constrained by tomography data, into a range dependent

85 ray code to isolate the last path detected in a full multipath pattern. Then, a representative  
86 group speed is solved for alongside position in a least squares fashion. This approach is able  
87 to re-position a floating hydrophone array with an error of 58 m and a standard deviation  
88 of 32 m based on six sources 129–450 km away but remains to seen for real-time navigation.

89 The ICEX20 AUV deployment necessitated an environmentally- and physically-driven  
90 relationship between recorded travel times and estimated pseudoranges due to the multipath  
91 uncertainty brought upon by an increasingly observed double ducted environment in the  
92 Beaufort Sea, which some refer to as the “Beaufort Lens” (Chen *et al.*, 2019; Chen and  
93 Schmidt, 2020; Litvak, 2015).

94 Given that a lens introduces significant ray refraction, the Beaufort Lens is a shorthand for  
95 the spatio-temporal variability of the local temperature and sound speed maxima generally  
96 around 50 to 60 m in depth. A neutrally buoyant layer of warm Pacific Summer Water  
97 creates a unique double ducted environment —the upper duct degrades signal coherence  
98 due to intensified ice interaction and the lower duct effectively traps sound for long range  
99 propagation (Poulsen and Schmidt, 2017). Modeling output (Duda *et al.*, 2021, 2019) and  
100 experimental observations (Ballard *et al.*, 2020; Bhatt, 2021) suggest that, in the Beaufort  
101 Sea, the duct is persistent and widespread but not necessarily continuous; it and its acoustic  
102 effects can be non-existent, minimal, or drastic. Transmissions in the upper duct, between  
103 the surface ice and the lens, experience minimal attenuation but degrade in signal coherence  
104 with repeated reflections under the ice. In lower duct, between the lens and its conjugate  
105 depth in the Atlantic water, roughly 200 m, sound above 350 Hz is trapped near losslessly  
106 for long range propagation (Poulsen and Schmidt, 2017).

107 Thorough reviews of uncrewed vehicle operations in polar environments can be found in  
108 (Norgren *et al.*, 2014) and (Barker *et al.*, 2020); there is no comparable work in the Arctic  
109 for a short range AUV deployment in the Beaufort Lens. Seminal (Bellingham *et al.*, 1995;  
110 Brooke, 1981; Hayes and Morison, 2002; Jackson, 1983; Light and Morison, 1989) and more  
111 recent AUV deployments (Fossum *et al.*, 2021; Jakuba *et al.*, 2008; Kukulya *et al.*, 2010;  
112 Kunz *et al.*, 2008; Plueddemann *et al.*, 2012; Timmermans and Winsor, 2013) witnessed the  
113 classical upward refracting sound speed profile that is amenable to an isovelocity assumption.

114 Of note, despite different platforms and scales, are recent glider deployments in the  
115 Canada Basin. In 2014, in partially ice-covered conditions, a long range LBL system with  
116 WHOI Micro-Modems at 100 m exploited the lower duct for long range communication with  
117 two gliders (Freitag *et al.*, 2016; Webster *et al.*, 2015). The sound speed value measured at  
118 the time of reception was used to estimate pseudorange in post-processing. The beacon-to-  
119 beacon performance was excellent, achieving contact at ranges greater than 200 km with  
120 a position uncertainty of 40 m. The beacon-to-glider performance, however, deteriorated  
121 due to missed contacts outside the duct, and was not described quantitatively. In 2017,  
122 gliders were deployed in a region with no ice coverage (Graupe *et al.*, 2019). Ranges were  
123 linearly scaled by a statistical description of sound speed observations taken during the  
124 experiment,  $1450 \pm 6.5$  m/s. This resulted in an error of 550 m, which was reduced by  
125 a factor between 4 and 5, depending on the dive, using a post-processing acoustic arrival  
126 matching method. Both cases exploit the lower duct for high fidelity communication at  
127 long ranges. Unintuitively, the smaller nature of our deployment during ICEX20 is not a

<sup>128</sup> simplifying factor. For source depths typical to vehicle operations, 30 to 200 m, a shadow  
<sup>129</sup> zone spans from 2 to 6 kilometers in range ([Schmidt and Schneider, 2016](#)).

<sup>130</sup> Compared to the previous small scale navigation efforts, the approach in this paper  
<sup>131</sup> integrates real-time model-aided data processing to estimate a representative sound speed  
<sup>132</sup> along a path from source to receiver, leveraging climatology, *in situ* data, and fast acoustic  
<sup>133</sup> modeling. The paper is organized as follows. Section [II](#) details the experimental approach  
<sup>134</sup> and conditions during ICEX20. Given that there is no GNSS ground truth for the vehicle  
<sup>135</sup> position while underway, we first evaluate the real-time ranging performance of GPS-linked  
<sup>136</sup> beacon-to-beacon communication events in section [III](#). Section [IV](#) uses insights from field  
<sup>137</sup> data to introduce a new ray filtering algorithm to improve range estimation. Section [V](#)  
<sup>138</sup> emulates the real-time processing pipeline to re-position beacon-to-beacon events and re-  
<sup>139</sup> navigate AUV *Macrura*.

<sup>140</sup> **II. OVERVIEW OF THE ICEX20 EXPERIMENT**

<sup>141</sup> The results from this paper derive from data taken while deploying the AUV *Macrura*, a  
<sup>142</sup> custom Bluefin-21, during the Ice Exercise 2020 (ICEX20), in the Beaufort Sea, from March  
<sup>143</sup> 8th to 11th. The AUV deployment was supported by the Integrated Communication and  
<sup>144</sup> Navigation Network (ICNN) ([Randeni et al., 2020, 2021; Schneider et al., 2020](#)), a special-  
<sup>145</sup> ized implementation of the LBL solution. The ICNN was initially developed via numerous  
<sup>146</sup> virtual experiments to ensure robust algorithms and interfaces between different hardware  
<sup>147</sup> components. The simulation capabilities are largely physics-driven with a modular system of  
<sup>148</sup> systems approach—an environmental simulator with sub-components for the ocean, includ-  
<sup>149</sup> ing Arctic ice drift and ocean acoustic propagation; a vehicle simulator with sub-components  
<sup>150</sup> for vehicle dynamics and navigation; a topside hardware simulator and acoustic communica-  
<sup>151</sup> tions simulator, both with a software-only configuration and a hardware-in-the-loop version  
<sup>152</sup> ([Schneider and Schmidt, 2018](#)). The virtual environment similarly emulates the interfaces  
<sup>153</sup> between the real components to test the entire software pipeline.

<sup>154</sup> **A. The Integrated Communication and Navigation Network**

<sup>155</sup> The ICNN is comprised of four ice buoys in a loose rectangle, roughly 2 km away from  
<sup>156</sup> a central ice camp with a topside computer, as shown in Fig. 1. The AUV and each ice  
<sup>157</sup> buoy are outfitted with a WHOI Micro-Modem ([Singh et al., 2006](#)), with a four-element  
<sup>158</sup> receiver array, a single transmitter, and one-tenth of a millisecond resolution. Acoustic  
<sup>159</sup> messages were sent with a 10 kHz carrier frequency, 5 kHz bandwidth, and phase-shift

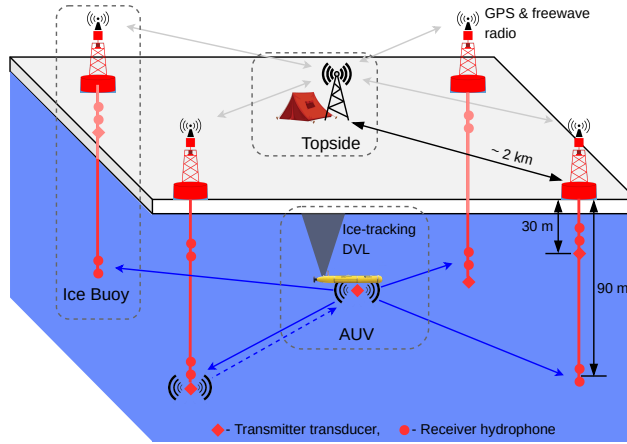


FIG. 1. A schematic overview of the Integrated Communication and Navigation Network (ICNN), which provides joint data-transfer and tracking between AUV and a human decision maker at Topside.

keying (PSK)modulation on a time-division multiple access schedule with a thirty-second cycle, giving room for two-way communication throughout the mission volume. The receive and transmit elements were split between shallow and deeper depths—30 and 90 m—to provide better coverage across the shadow zone. While each buoy only has one transmit depth, all buoys have both receive depths but the active receive layer is consistent across all buoys. The design of the ICNN enables a self-adapting network to transmit and receive at the optimal depth to maintain contact with the AUV (Schneider *et al.*, 2020). The buoys do not encompass the full horizontal range of the vehicle but are positioned to minimize overlap in trilateration for spherical positioning (Deffenbaugh *et al.*, 1996a).

To balance competing uses of the acoustic channel, the network uses a single synchronized digital communication packet to provide both tracking and data to the operator.

171 1. The AUV, running an ice-tracking DVL and an onboard hydrodynamic model, broad-  
172 casts its perceived location on a scheduled, time-synchronized message via WHOI  
173 Micro-Modem

174 2. Four ice buoys, each outfitted with a WHOI Micro-Modem, receive messages from the  
175 AUV and send that information over freewave radio to a Topside computer

176 3. The topside computer converts travel times into pseudorange estimates using a stochas-  
177 tic embedded prediction of the horizontal group velocity via BELLHOP ray tracing  
178 code ([Porter, 2011](#)) using a sound speed profile provided by an updatable Virtual  
179 Ocean ([Bhatt \*et al.\*, 2022; Schneider and Schmidt, 2018](#))

180 4. The topside computer calculates a new position by trilaterating the range estimates

181 5. The position differential, not the absolute position, is broadcast to the vehicle to  
182 update its navigation solution and be robust to latency and intermittency

183 In the face of GNSS-denied navigation, this approach was anecdotally successful, as shown

184 in Fig. 2. The AUV *Macrura* was deployed through a hydrohole from an ice camp but re-

185 covered through an emergency hydrohole. A random disk error stalled *Macrura* underneath

186 the ice but did not prevent it from transmitting its location. Due to an incoming storm, a

187 team placed a physical marker on the ice at the location. Three days later, *Macrura* was

188 found within a meter of the marker. We view the emergency recovery as qualitative proof

189 of the robustness of this navigation approach. Nonetheless, this paper specifically addresses

190 the third and fourth steps—the conversion of travel times into pseudoranges and its effect

191 on trilateration. By focusing on pseudorange estimates between GPS-tracked beacons, and

re-running the trilateration pipeline, the results are decoupled from all other mechanisms in the ICNN.

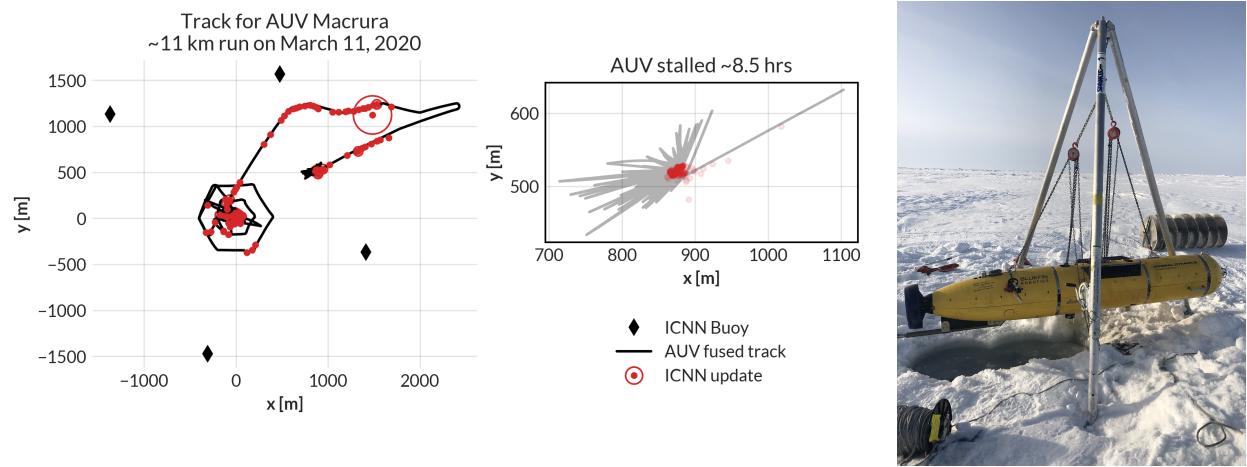


FIG. 2. The under-ice mission track for AUV *Macrura*, including the position updates as it stalled underneath the ice overnight. A marker was placed on the ice at the vehicle’s estimated self-location. It was recovered after a three day storm within a meter of the marker.

## 194 B. ICEX20 sound speed conditions

An important component to our navigation solution is an accurate estimation of a representative SSP for the ocean volume. Previous field experience, during the Ice Exercise 2016 (ICEX16), demonstrated the negative effects of the Beaufort Lens on tracking and communication (Schmidt and Schneider, 2016). Fig. 3 shows historical, modeled, and *in situ* sound speed data for both ICEX16 and ICEX20. These three input streams were selected to mirror the information available on a submarine (personal conversation with LT B. Howard and LT CDR D. Goodwin). In the field, the SSP information was shared with the vehicle via basis

representation compression on a lightweight digital acoustic message (Bhatt *et al.*, 2022). All modeled data comes from HYCOM (Chassignet *et al.*, 2007), which does not seem to capture the forcing mechanisms that cause the Beaufort Lens. For ICEX16, the data-driven profile was sourced from nearby Ice Tethered Profilers (ITP) after the field experiment (Krishfield *et al.*, 2008; Toole *et al.*, 2011) and exhibits a fairly low lens; the historical profile is from the World Ocean Atlas. For ICEX20, the chosen weights (data-driven) profile derives from an estimate of initial CTD casts taken on site, showing an intense warm water intrusion; the baseline (historical) profile, showing moderate ducted conditions, comes from the average of March 2013 ITP data. This month best matched sea ice and sound speed conditions at the beginning of ICEX20 (Bhatt *et al.*, 2022). It is important to note that all profiles that do show the Beaufort Lens do so with different local sound speed maxima at different depths, reflective of the wide range of lens properties observed for all ITP data in the region. The variability of the lens height and prominence is the main reason an updatable SSP was integrated into the ICNN solution.

During ICEX20, the HYCOM profile was available but never deployed. For post-processing comparison, we introduce both the HYCOM profile and an isovelocity case,  $1441.8 \pm 3.7$  m/s, as the mean and standard deviation of the observed sound speed profile over the first 200 m.

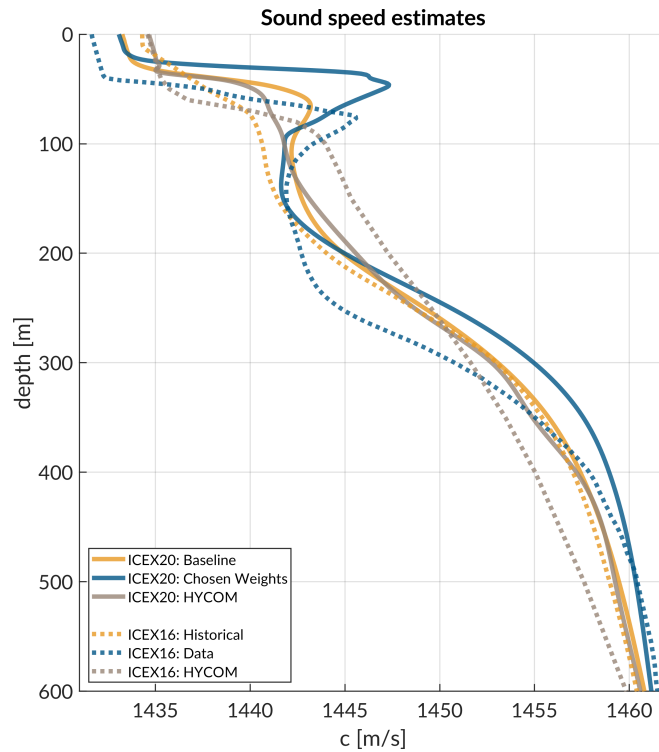


FIG. 3. Sound speed conditions for historical (baseline), data (chosen weights), and HYCOM model for both ICEX16 and ICEX20.

220 **III. REAL-TIME PSEUDORANGE ANALYSIS**

221 Because the vehicle's navigation solution during a mission can only be evaluated on the  
222 basis of the error estimates sent, a sister experiment for validating the real-time ranging  
223 approach was implemented. Ice buoy modems were run as "virtual vehicles" at a fixed  
224 depth, receiving position updates from the other beacons as well as a camp site modem  
225 lowered to 20 m. Figure 4 shows successful events sorted by source depth. In this analysis,  
226 we assume there is insignificant displacement between the GNSS puck surface expression and  
227 subsurface modem; this is supported by unusually low observed ice drift rates, on average,  
228 just 0.7 cm/s.

229 **A. Minimal bounce criteria (MBC)**

230 The fundamental challenge to implement GNSS-like navigation, especially in an acousti-  
231 cally complex propagation environment, is characterizing a single sound speed to compensate  
232 for the effects of ray refraction and reflection. The use of the acoustic modem network for  
233 tracking relies on the accurate estimates of travel times between the submerged platform  
234 and LBL beacons, supported by clock synchronization and a pre-determined scheduling of  
235 acoustic events. For the Beaufort Lens in particular, the strong multipath effects make it  
236 virtually impossible to deterministically predict the modem's detected arrival time.

237 Instead, for each individual modem  $i$ , an embedded stochastic tracking framework is used  
238 to provide a running estimate of the horizontal group velocity  $u_{i,j}$  for the conversion from  
239 travel time to range from modem  $j$ , with the ultimate goal of matching the naive group

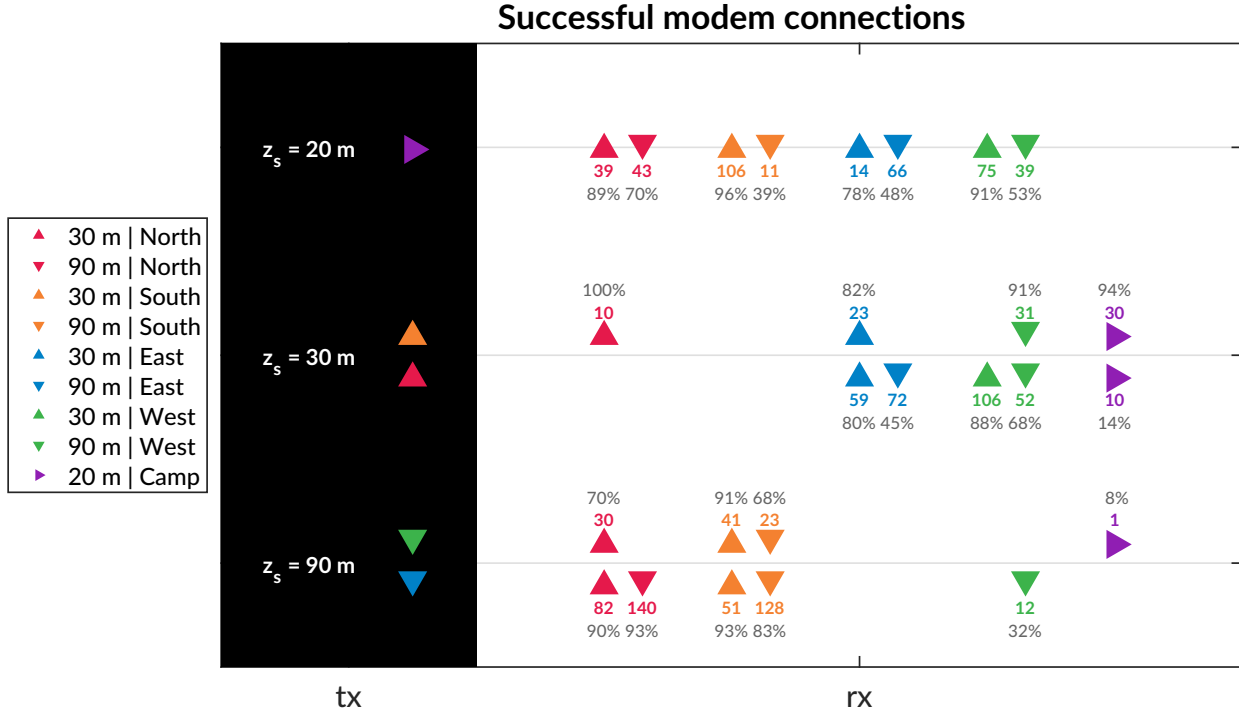


FIG. 4. An overview of the modem experiment by source and receiver depth and position with the number of successful decodings and the percent success rate, defined as the ratio of decoded to detected. The black column on the left, *tx*, shows the source depth,  $z_s$ . The column on the right, *rx*, shows the receivers with the amount of good contacts. The orientation of the triangles—sideways, upwards, and downwards—corresponds to depths of 20, 30, and 90 m.

240 velocity, i.e. the GPS-recorded distance between two nodes divided by the modem-recorded  
241 one way travel time between them.

242 In the ICEX20 configuration, the acoustic tracking is running on the topside computer,  
243 which controls the ICNN. Here we assume that the group velocities  $u_{i,j}$  are smoothly varying  
244 over the course of a vehicle mission, i.e., with respect to range, mission time, and the

<sup>245</sup> frequency of updates relative to vehicle motion. The group velocity is tracked on a thirty-  
<sup>246</sup> second cycle using predictions from the *Virtual Ocean* infrastructure.

<sup>247</sup> When the topside tracking framework receives a modem message, with a time delay,  $\Delta t$ ,  
<sup>248</sup> from one of the range modems, it will request a new estimate of the group velocity and its  
<sup>249</sup> associated uncertainty. The group velocity estimate is found using the vehicle's reported  
<sup>250</sup> depth and the extrapolated navigation solution for range,  $\hat{r}$ , as inputs for the ray tracing  
<sup>251</sup> program. The latter returns an impulse response estimate in the form of ray travel times  
<sup>252</sup>  $dt_j$  and amplitudes  $a_j$  for that range and depth.

<sup>253</sup> The initial call to BELLHOP is over a local grid centered at the range and depth posited  
<sup>254</sup> by the onboard tracking solution. The grid, compared to a point solver, adds redundancy in  
<sup>255</sup> resolving the actual multipath structure for a reliable acoustic path without taxing onboard  
<sup>256</sup> computational time and memory. It is initialized as  $11 \times 11$  points spanning 10 m horizontally  
<sup>257</sup> and 20 m vertically. The horizontal dimension reflects the accumulated position error given  
<sup>258</sup> a thirty-second communication cycle; the vertical dimension reflects how, computationally,  
<sup>259</sup> eigenrays of the same timefront seem to stack vertically in the water column. For each  
<sup>260</sup> grid point, BELLHOP produces a number of arrivals resulting from multiple propagation  
<sup>261</sup> paths for any source-receiver pair. Using only the  $N_0$  rays with neither surface nor bottom  
<sup>262</sup> bounces, it will then estimate the current group velocity  $u$  from a power weighted average  
<sup>263</sup> of the ray travel times,

$$u = \frac{\hat{r} \sum_{n=1}^{N_0} a_n^2}{\sum_{n=1}^{N_0} dt_n a_n^2}, \quad (1)$$

<sup>264</sup> and the associated weighted standard deviation,

$$\sigma_u \simeq \sqrt{\frac{\sum_{n=1}^{N_0} (dt_n - \hat{r}/u)^2 a_n^2}{\sum_{n=1}^{N_0} a_n^2}} \frac{u^2}{\hat{r}} \quad (2)$$

<sup>265</sup> If no direct paths exist, i.e.  $N_0 = 0$ , then the group velocity is computed using the same

<sup>266</sup> algorithm for the ray arrivals with one bounce, and so on.

<sup>267</sup> Finally, the pseudorange is calculated simply as

$$r_{i,j} = u_{i,j} \Delta t_{i,j} \quad (3)$$

<sup>268</sup> Thus the NBC method assumes the signal detected by the modem will be dominated

<sup>269</sup> set of paths with the least number of boundary interactions. Importantly, this stochastic,

<sup>270</sup> ensemble method for group velocity calculation can run in real-time, appearing to be orders

<sup>271</sup> of magnitude faster than other post-processing methods which seek to determine the specific

<sup>272</sup> ray itself that best matches a prominent indicator from the arrival structure. The BELLHOP

<sup>273</sup> simulation that runs this calculation uses 3600 rays with launch angle fan of -60 to 60 degrees,

<sup>274</sup> a representative depth dependent sound speed profile, and a range dependent bathymetry.

<sup>275</sup> **B. Pseudorange error metrics**

<sup>276</sup> The sister modem experiment generated 811 beacon to beacon communication events with

<sup>277</sup> their own real-time MBC group velocity predictions. Given the complexity of the ICNN

<sup>278</sup> system, this experiment did not collect an exhaustive set of data across all buoy, source

<sup>279</sup> depth, receive depth, and sound speed combinations. The algorithm generally overestimates

<sup>280</sup> pseudoranges because it resolves the effective sound speed for the most direct path.

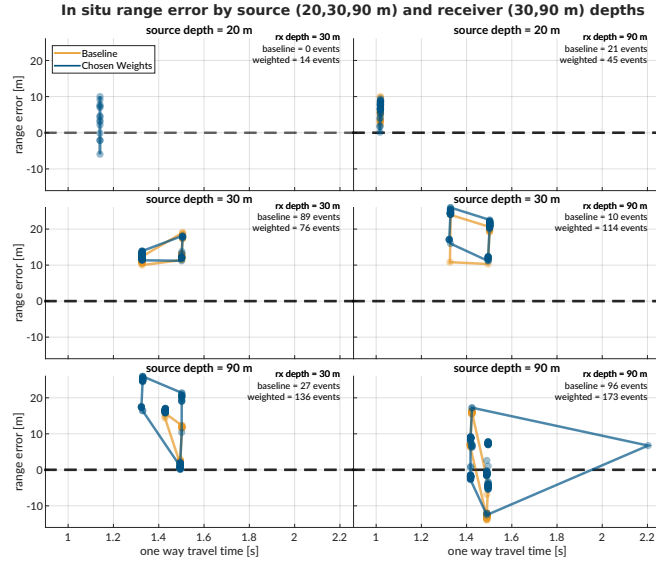


FIG. 5. The real-time range error by source (20, 30, and 90 m) and receiver (30 and 90 m) pairings for both sound speed estimates used during ICEX20. The amount of communication events is notated in the top right of each panel. The dashed line indicates no range error, and the boundary drawn indicates scope of the range error as a function of one way travel time.

281     Figure 5 shows the range error boundary for both SSP inputs used in ICEX20. A promising sign that the MBC method adapts sound speed realistically is no obvious error growth  
 282     as travel time increases. The baseline SSP ( $n=243$  events) has an absolute pseudorange  
 283     error of  $11.38 \pm 4.23$  m; the weighted SSP ( $n=568$ ),  $11.36 \pm 8.12$  m. The discrepancy  
 284     between these two is largely due to outlier events only contained in the weighted SSP set.  
 285  
 286     Where there is overlap between sound speed conditions used for the real-time MBC, the  
 287     pseudorange error difference is no more than a few meters. The overarching results show  
 288     that sound speed estimates derived from eigenrays for a local grid, as opposed to a singular  
 289     point, are accurate enough to support vehicle navigation. While the NBC looks for just the  
 290     least complex multipath, the high density of launch angles almost always guarantees a direct

<sup>291</sup> path. Nonetheless, the consistent overestimation of pseudorange invites further analysis into  
<sup>292</sup> acoustic arrival matching.

<sup>293</sup> **C. Eigenray identification for beacon-to-beacon events**

<sup>294</sup> Accounting for ice movement between beacons creates nominal ranges with small variabil-  
<sup>295</sup> ity. Figs. ?? each show eigenrays for three sound speed environments for source depths of  
<sup>296</sup> 20, 30, and 90 m, respectively. Eigenrays were initially found using the built-in BELLHOP  
<sup>297</sup> protocol with a launch angle step of 0.05 degrees from -60 to 60 degrees. Separately, recorded  
<sup>298</sup> travel times between beacons were clustered with 1 millisecond boundaries such that some  
<sup>299</sup> source-receiver pairs had multiple, distinct travel times to approximate. The BELLHOP  
<sup>300</sup> eigenray returns were then filtered such that one was selected per travel time cluster, in the  
<sup>301</sup> hopes that the eigenray will converge to the receiver locations for the most realistic sound  
<sup>302</sup> speed input. It should be noted that bottom bounces were recovered but filtered out. The  
<sup>303</sup> three source depths create distinguishable ray geometries with respect to the three sound  
<sup>304</sup> speed inputs.

<sup>305</sup> **1. Source depth of 20 m**

<sup>306</sup> For a source at 20 m in depth, shown in Fig. 6, reliable eigenrays are found for all sound  
<sup>307</sup> speed inputs. Rays refract upwards and neatly intersect with the shallow and deep receiver  
<sup>308</sup> locations between 1.5 and 1.8 km in range. However, the ray paths for the shallow receivers  
<sup>309</sup> change both in the number of surface interactions and where the surface interactions occur  
<sup>310</sup> with respect to range across the SSPs. As the Beaufort Lens strengthens, the chosen paths to

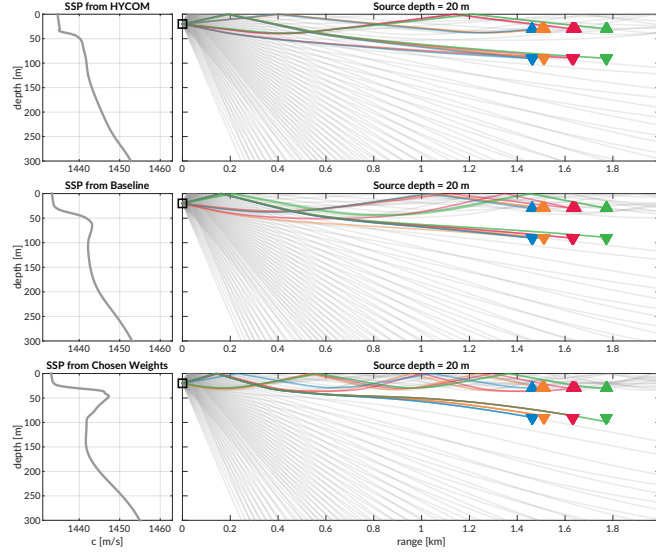


FIG. 6. Eigenrays for beacon to beacon events for each sound speed with a nominal source depth of 20 m. The beacons are highlighted in color/marker coding in Fig. 4. The eigenrays are curated from BELLHOP by travel time proximity and are traced in the representative receiver colors over a total ray fan in gray.

311 the second farthest shallow buoy (North, in red) interact with the surface more and become  
 312 distinct. The weighted SSP shows the most interesting effects for the deeper receivers. The  
 313 ray paths all interact with the surface and the eigenrays for the Northern (red) and Western  
 314 (green) buoys are in fact the same ray.

315 **2. Source depth of 30 m**

316 The ray geometries from the 30 m source, shown in Fig. 6, show a similar degradation  
 317 of eigenray identification with increased ducting. Receptions span 1.5 to 3.2 km. Once  
 318 again, eigenrays for HYCOM and the baseline SSP are visually appropriate. Rays for the  
 319 weighted SSP show how the surface channel intensifies ice interactions and how the shadow

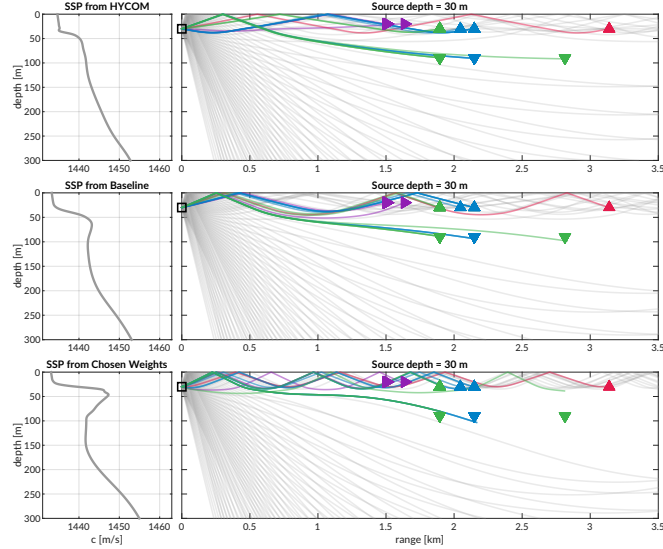


FIG. 7. Eigenrays for beacon to beacon events for each sound speed with a nominal source depth of 30 m. The beacons are highlighted in color/marker coding in Fig. 4. The eigenrays are curated from BELLHOP by travel time proximity and are traced in the representative receiver colors over a total ray fan in gray.

320 zone denies reliable acoustic paths. Pointedly, the increasing number of surface reflections to  
 321 the farthest shallow buoy (North, in red) crystallize the MBC's tendency for overestimation.  
 322 For the HYCOM, baseline, and weighted SSP inputs, the most appropriate eigenrays show  
 323 2, 3, and 4 surface interactions.

324 ***3. Source depth of 90 m***

325 Lastly, Fig. 8 shows ray geometries from the 90 m source, elucidating a different extent  
 326 of the shadow zone. While the receiver locations are similar to that of the 30 m source  
 327 depth, the deeper source depth effectively negates the upper duct and places the upper (and  
 328 some of the lower) receivers in unreliable acoustic paths. The HYCOM eigenrays still show

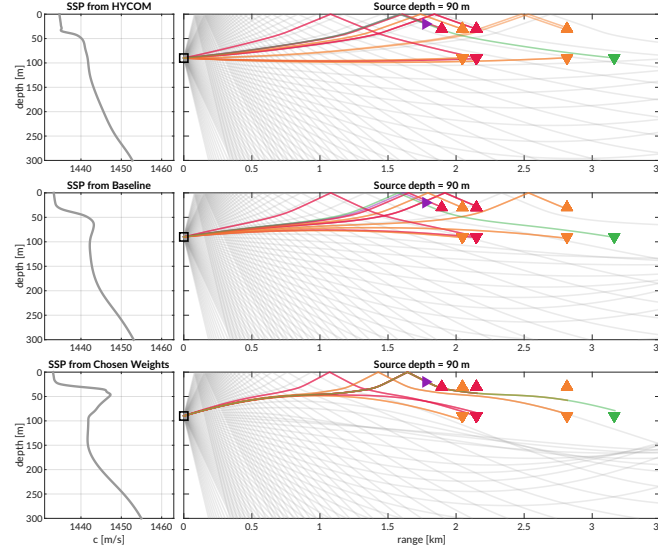


FIG. 8. Eigenrays for beacon to beacon events for each sound speed with a nominal source depth of 90 m. The beacons are highlighted in color/marker coding in Fig. 4. The eigenrays are curated from BELLHOP by travel time proximity and are traced in the representative receiver colors over a total ray fan in gray.

329 the most reliable acoustic paths that deteriorate with increasing ducted conditions. The  
 330 lack of direct paths from the observed SSP further points out the shortcomings of the MBC  
 331 approach.

332 The goal of the MBC algorithm was to provide a reliable, physically intuitive interpre-  
 333 tation of the acoustic propagation without taking on the additional burden of regularly  
 334 identifying specific paths that may connect any given source-receiver pair in the network.  
 335 Its performance was adequate for vehicle navigation and would have likely sufficed if it were  
 336 not for the prominence of the duct observed relative that of other model and data products.

337

<sup>338</sup> **IV. POST-PROCESSED PSEUDORANGE ANALYSIS**

<sup>339</sup> From all events recorded during the modem test experiment, there are 1242 successfully  
<sup>340</sup> decoded beacon-to-beacon events. Only these events are used to evaluate ranging accuracy,  
<sup>341</sup> as the ICNN was not configured to use receptions with failure flags. Thus, a post-processing  
<sup>342</sup> analysis that emulates the real-time navigation engine was run to overcome the unequal  
<sup>343</sup> distribution of communication events with respect to depth, range, and sound speed status.

<sup>344</sup> It is important to note that the value for the extrapolated range,  $\hat{r}$ , is only tracked when  
<sup>345</sup> the modem runs the vehicle behavior; thus we replace  $\hat{r}$  with the GPS-tracked range for all  
<sup>346</sup> modem events. Because  $\hat{r}$  converges to the correct solution, a comparison of  $\hat{r}$  with the GPS-  
<sup>347</sup> tracked range shows a normal, zero-centered distribution within the bounds of GPS drift.

<sup>348</sup> The present analysis therefore seeds realistic but “omniscient” knowledge of the extrapolated  
<sup>349</sup> range and leverages the post-processing pipeline to more thoroughly evaluate the acoustic  
<sup>350</sup> range estimate for all modem events, with three relevant sound speed sources, and both  
<sup>351</sup> group velocity criterion. Accordingly, the results in this section evaluate the utility of the  
<sup>352</sup> algorithms and sound speed sources, divorced from their role in the ICNN while maintaining  
<sup>353</sup> real-time relevance.

<sup>354</sup> **A. Nearest bounce criteria (NBC)**

<sup>355</sup> As shown in the eigenray traces of Fig. 7, the extent of ray bending and repeated  
<sup>356</sup> reflections is extremely dependent on the sound speed profile. An isovelocity approach  
<sup>357</sup> would completely miss this nuance; our field-tested approach that only resolved the simplest

358 path is unlikely to resolve the one that triggers modem detection. Based on this insight, a  
 359 new algorithm, the nearest bounce criteria (NBC), is a slight modification from the MBC  
 360 and includes multipath as a new dimension of information to exploit. This metric, while  
 361 run in post-processing, adds a negligible amount of computation for real-time efficacy.

362 Given a running estimate for the horizontal group velocity  $u_{i,j}$  between nodes  $i$  and  $j$ ,  
 363 the navigation system has an extrapolated value for range,  $\hat{r}$ , and a recorded travel time,  
 364  $\Delta t_{i,j}$ . Instead of using only the  $N_0$  rays with neither surface nor bottom bounces to estimate  
 365 group velocity and subsequently moving to incremental number of bounces only when no  
 366 valid direct path solutions exist, we solve for the power weighted average of the ray travel  
 367 time for the  $N_k$  rays with  $k$  bounces,

$$t_k = \frac{\sum_{n=1}^{N_k} dt_n a_n^2}{\sum_{n=1}^{N_k} a_n^2}, \quad (4)$$

368 find the nearest matching power weighted average to recorded travel time,

$$t_{i,j,k} = \min_{k=0,1,2,\dots} |t_k - \Delta t_{i,j}| \quad (5)$$

369 predict a group velocity,

$$u_{i,j} = \frac{\hat{r}}{t_{i,j,k}} \quad (6)$$

370 and estimate the range as was done previously.

$$r_{i,j} = u_{i,j} \Delta t_{i,j} \quad (7)$$

371 This method selects a different group velocity based on the multipath arrival structure,  
 372 as the detected arrival is not always the first arrival or the direct path and could even be  
 373 masked by noise or blocked temporarily (Deffenbaugh *et al.*, 1996b). We manually cap the

<sup>374</sup> number of bounces to 4 because of the smaller operational scale and the attenuation accrued  
<sup>375</sup> with many surface interactions. Bottom bounces are not encoded separately because of ray's  
<sup>376</sup> tendency to refract upward, not due to information limitations.

<sup>377</sup> **B. Effective sound speed predictions**

<sup>378</sup> The minimal and nearest bounce algorithms are applied with the three sound speed inputs  
<sup>379</sup> shown in Fig. 7. The resulting predicted group velocities for all source depths are shown in  
<sup>380</sup> Fig 9.

<sup>381</sup> The goal of the group velocity estimation is to converge towards the implied sound speed,  
<sup>382</sup> i.e. the GNSS-derived range divided by the recorded travel time. For a 30 m receiver depth,  
<sup>383</sup> the NBC shows more overlap with data-derived values as it classifies multipath more cor-  
<sup>384</sup> rectly. For a 90 m receiver depth, the overlap is less accurate due to computational con-  
<sup>385</sup> straints of a limited fan of rays entering the shadow zone rendering a less reliable simulated  
<sup>386</sup> times of arrival packet.

<sup>387</sup> As the environmental and ray filtering method become better representations of the real  
<sup>388</sup> ocean, the lower the expected mismatch is between the implied and estimated effective  
<sup>389</sup> sound speeds. Analysis shows that the higher multipath classification produces more ac-  
<sup>390</sup> curate sound speed predictions, likely driven by a tighter and/or sparser bundle of rays.  
<sup>391</sup> However, that data are too small to draw significant conclusions. Discontinuities in mul-  
<sup>392</sup> tipath classification verify our hypothesis for its importance to a smoothly varying group  
<sup>393</sup> velocity, as shown in the cluster for a receiver depth of 30 m, where HYCOM jumps from

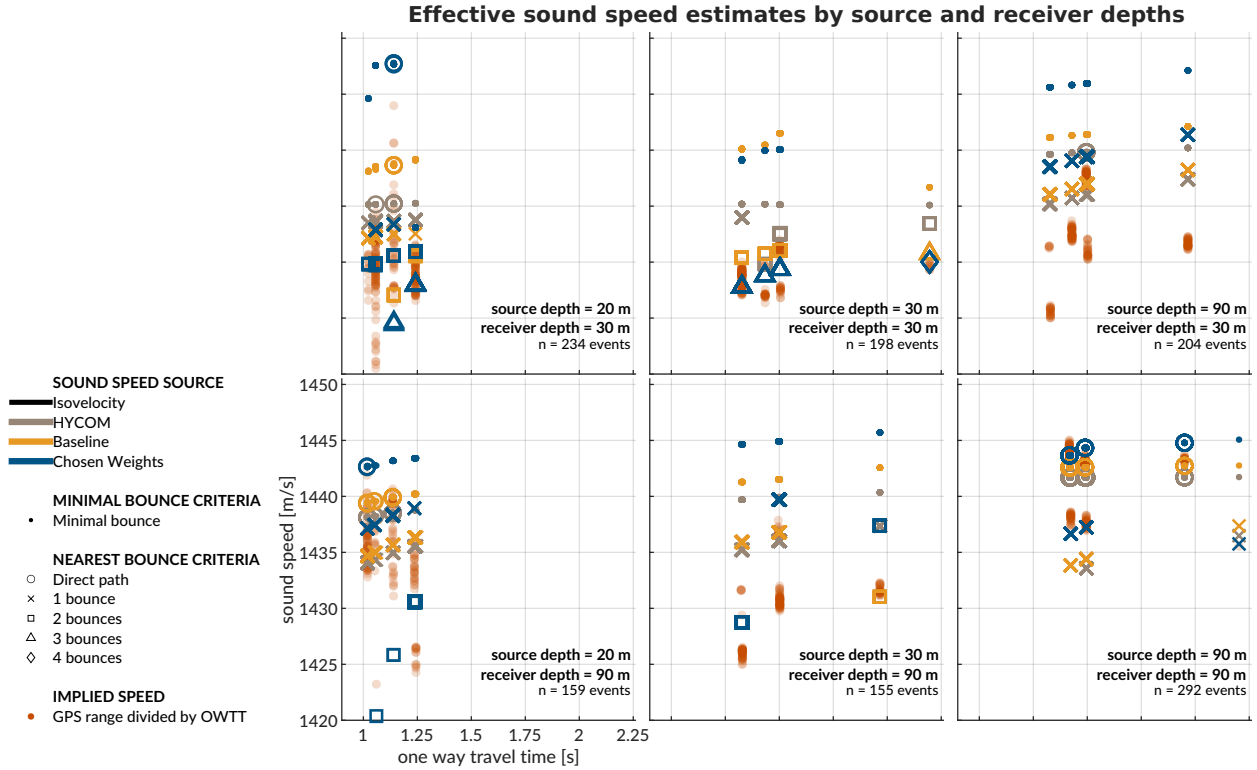


FIG. 9. A comparison of group velocity predictions for all beacon to beacon events in post-processing with a source depth of 30 m, with group velocity on the y-axis and recorded travel time on the x-axis. The left panel is for a receiver depth of 30 m; the right panel for 90 m. The sound speed source is indicated by color. The minimal and nearest bounce criterion are distinguished by different marker shapes, compared to the separately colored red dots showing the naive, data-driven group velocity calculation.

394 one to two bounces amidst the baseline SSP and weighted SSP smoothly increasing while  
 395 consistently seeing two and three bounces, respectively.

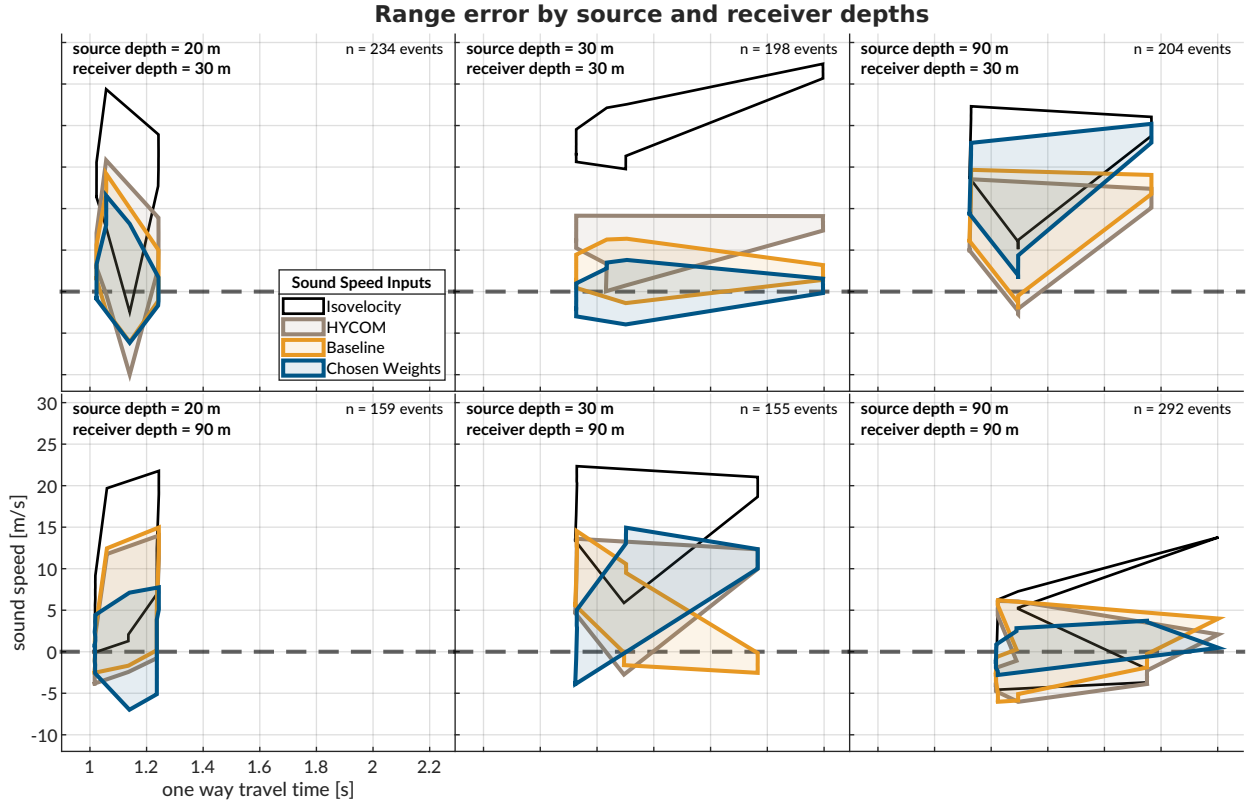


FIG. 10. The post-processed range error for source depths of 20, 30, and 90 m, and receiver depths of 30 and 90 m. The dashed gray line shows no error. The shaded region connects the range performance across all events.

**396 C. Pseudorange error metrics**

**397** Fig. 10 shows the directional range error footprints for all three sound speed inputs with  
**398** respect to OWTT, separated by source and receiver depth configurations. The weighted  
**399** SSP range error generally has the smallest and most zero-centered footprint. The one case  
**400** it does not is for the source-receiver pairings between 30 and 90 m in depth. The increased  
**401** error for these reciprocal transmission paths is most likely driven by the computational  
**402** artifacts encountered when propagating through the steep sound speed gradients of the lens

403 and through the shadow zone. All other source depth pairings are significantly improved  
 404 using the chosen weights compared to HYCOM or the baseline.

405 When using a linear scaling to convert travel time into range, any offset between the  
 406 assumed sound speed and the horizontal group velocity produces unconstrained error with  
 407 increasing receiver distance. Most importantly, we see the consequences of the adaptive  
 408 group velocity in that range error does not strictly increase with OWTT.

409 The improvement from MBC to NBC is most evident for the realistic sound speed; while  
 410 the HYCOM SSP improves from a median absolute range error of 6.41 to 4.61 m, the  
 411 baseline SSP improves from 10.30 to 2.27 m, and the weighted SSP improves from 13.28  
 412 to 2.12 m. Table I shows further statistics on the absolute range error by SSP and group  
 413 velocity algorithm. The order of magnitude improvement in the ducted SSPs demonstrate  
 414 the effectiveness of the algorithm exploiting the multipath conditions.

415 As shown in table I, there is a striking maximum range error of 1491 m for the weighted  
 416 SSP in the minimal bounce criteria. There are 10 events from South transmitting at 30 m  
 417 depth to North receiving at 30 m depth. The OWTT spread is from 2.1958 to 2.1963 s; the  
 418 naive group velocity is 1429.3 to 1430.1 m/s; and the GPS-tracked range is from 3138.54 m  
 419 to 3140.87 m. This example ends up being an excellent case study for how sound speed and  
 420 multipath fidelity work in concert to minimize range error. The large error in this instance  
 421 is driven by the MBC unexpectedly defaulting to a bottom bounce with a much greater  
 422 OWTT. The NBC classifies the multipath as 4 bounces, reducing the range error from  
 423 greater than a kilometer to less than a meter. While there is no actual way of knowing if  
 424 this is the correct multipath structure, the range error is remarkably small, at 0.025%. This

	Baseline		Chosen Weights		HYCOM	
	MBC	NBC	MBC	NBC	MBC	NBC
minimum [m]	0.01	0.00	0.00	0.00	0.11	0.01
25th % [m]	4.96	0.99	6.26	0.95	3.30	2.25
median [m]	10.30	2.27	13.28	2.12	6.41	4.61
75th % [m]	15.81	5.51	19.75	4.11	10.92	7.46
maximum [m]	22.52	14.96	1491	20.21	19.55	15.81

TABLE I. A comparison of range estimation metrics for each sound speed source and group velocity estimation algorithm for all 1283 beacon to beacon events via post-processing. The 0th (minimum), 25th, 50th (median), 75th, and 100th (maximum) percentiles are shown to the range resolution afforded by the WHOI Micro-Modem. There are a few outliers that drive the mean to be higher than the median.

425 pattern of not choosing the minimal observed bounce structure is consistent across all SSPs;  
 426 the baseline goes from 1 to 3 bounces and HYCOM goes from 0 to 2 bounces. Notably,  
 427 the baseline and HYCOM range errors are never egregiously large, but are nonetheless  
 428 improved with the NBC algorithm. Thus, for acoustically complex environments, the NBC  
 429 has a disproportionately positive impact as the estimated SSP approaches the desired SSP.

<sup>430</sup> **V. TRILATERATION FOR ICEX20 FIELD DATA**

<sup>431</sup> To overcome potentially intermittent acoustic communication, the operational paradigm  
<sup>432</sup> of the ICNN computes corrections relative to the trilaterated position estimates transmitted  
<sup>433</sup> by the vehicle, rather than transmitting the updated positions themselves. The reliability  
<sup>434</sup> of the correction is directly linked to how accurately the travel time measurements are  
<sup>435</sup> converted to pseudoranges. This section aims to resolve that tension by reevaluating the  
<sup>436</sup> trilateration results with respect to the MBC and NBC algorithms. The MBC/NBC sound  
<sup>437</sup> speed estimates were tracked independently for each transmitter-receiver pair; although the  
<sup>438</sup> sound speed was expected to be locally smooth near a given receiver, no such assumption  
<sup>439</sup> was enforced between distinct acoustic links.

<sup>440</sup> **A. Re-positioning beacon to beacon events**

<sup>441</sup> When the beacons ran as virtual vehicles, the ICNN did not have access to that buoy's  
<sup>442</sup> GPS data stream except for what was sent via digital acoustic message. The static nature of  
<sup>443</sup> the experiment means that the initial estimate transmitted to the ICNN was in fact a ground  
<sup>444</sup> truth position. Therefore, a distribution of corrections from the ICNN, as shown in Fig. 11,  
<sup>445</sup> reflects positioning accuracy. The NBC clearly outperforms the MBC, with almost 80% of  
<sup>446</sup> the corrections below 6 meters and the median within the deployed GNSS puck precision  
<sup>447</sup> of 3 meters. By contrast, the MBC shows roughly 20% within the GNSS puck precision,  
<sup>448</sup> and separate peaks from 9–12 meters and 21–27 meters. This trimodal nature reflects the  
<sup>449</sup> distribution of reflections on the ice surface.

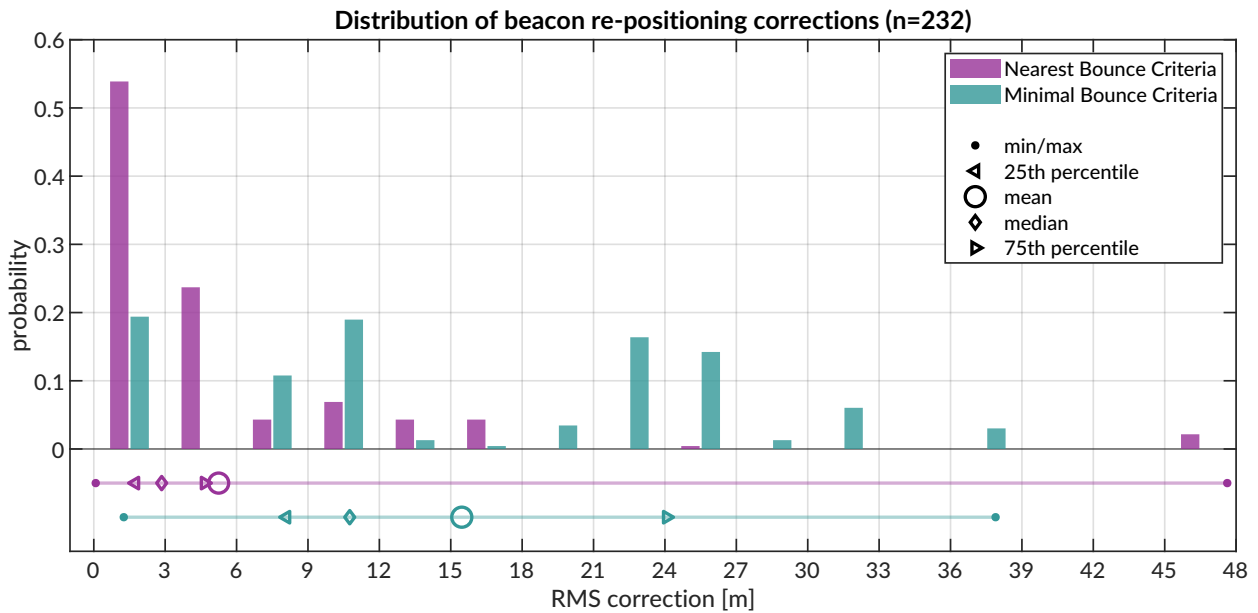


FIG. 11. Trilateration events; however, 264 entries are 2-beacon solutions, 22 are 3-beacon, and 2 are 4-beacon. When limited to only two ranging circles, the trilateration chooses the closer of the two intersection points. The x-axis is cut off at the upper limit for the NBC algorithm.

450 In several events, the MBC is unable to accurately estimate the effective sound speed for  
 451 one of the acoustic links, leading to a large positioning error. The NBC, however, better  
 452 resolves an approximation of the acoustic path. For example, in some trilateration solutions  
 453 for the Eastern buoy, the MBC shows a correction of more than a kilometer; the NBC is  
 454 two order of magnitudes less.

455 **B. Re-navigating AUV *Macrura***

456 Up to this point, pseudorange estimation and localization have been evaluated on GPS-  
 457 linked beacon-to-beacon connections to validate the NBC algorithm. This analysis ports the  
 458 MBC and NBC algorithms to re-navigate the AUV *Macrura*.

459        The AUV dataset clearly exhibits instances where a receiver detects the same transmission  
 460      more than once. This is not surprising considering the complex multipath provided by  
 461      the Beaufort Lens. The 11 hour vehicle mission contains 3260 transmissions, 12938 total  
 462      detections, and 4704 successful receptions. Allowing receptions with PSK errors would  
 463      almost double the number of recorded multipath arrivals exploited for positioning, if a real-  
 464      time solution could correctly parse paths from different arrivals in the same thirty-second  
 465      cycle. Thus it remains a future endeavor to explore how failure mode information from  
 466      acoustic modems could be used to identify unsuccessful but otherwise trustworthy arrivals  
 467      to augment trilateration samples.

468        The following performance analysis is constrained to what the vehicle acted on in real-  
 469      time. AUV *Macrura* and the ICNN ran an adaptive depth behavior to maintain acoustic  
 470      communication on the insight that cross-layer links were more likely to fail than same-layer  
 471      ones. Accordingly, the vehicle dove deeper than 50 meters about 20% of the time it was  
 472      underway.

473        In contrast to the modem tests, where position correction illustrated re-positioning ac-  
 474      curacy, the re-navigation corrections are less valuable in the absence of GNSS ground truth.  
 475       The correction magnitude necessarily depends on the vehicle's internal navigation estimate,  
 476      which is prone to larger errors from sensor drifts, ocean currents, and other error not cap-  
 477      tured in the hydrodynamic model. Thus, larger corrections are not necessarily indicative of  
 478      worse performance. Navigation accuracy may be better described by trilateration error, the  
 479      RMS of the remaining pseudorange errors from each acoustic link.

480 Fig. 12 shows the correction magnitudes and trilateration errors for events with three or  
 481 more receptions during AUV operations. Whereas the MBC has a fairly bimodal nature,  
 482 with peaks centered around 10–15 and 35–40 m, the NBC favors smaller corrections, from  
 483 5–20 m, and has a long tail. The distribution of corrections are much larger than the  
 484 distribution of RMS error. It is apparent that, while both methods are quite successful,  
 485 there is strong evidence that the NBC achieves single meter accuracy.

### 486 C. Investigating potential GNSS noise

487 The fact that the bulk of the best performing re-navigation error exists within the pre-  
 488 cision of the GNSS unit deployed invites a further look into GNSS noise. In the Arctic,  
 489 GNSS performance worsens due to poor constellation coverage, larger ionospheric effects,  
 490 and multipath interference. The National Security Implications of Climate Change for U.S.  
 491 Naval Forces (Council, 2011) details some of the limitations of the Global Positioning Sys-  
 492 tem (GPS) at polar latitudes. Radio infrastructure that provides position corrections and  
 493 references does not regularly extend to polar regions. The effect is minor for surface platform  
 494 navigation —roughly 15 m of horizontal precision has been displayed at the North Pole—but  
 495 is significant enough to register against the modem’s detected travel times. Figure 13 zooms  
 496 in on the GNSS and OWTT noise relative to the ice movement for two pairs of modem buoy  
 497 connections. The two panels indicate the GPS drift as  $\delta R = \sqrt{\delta x^2 + \delta y^2}$  and temporal drift,  
 498  $\delta t$ , relative to the median OWTT recorded between the two modems. The dashed line is  
 499 scaled by a group velocity of 1440 m/s, such that if there were ideal sensor measurements  
 500 with no drift, all events should exist on or near the line.

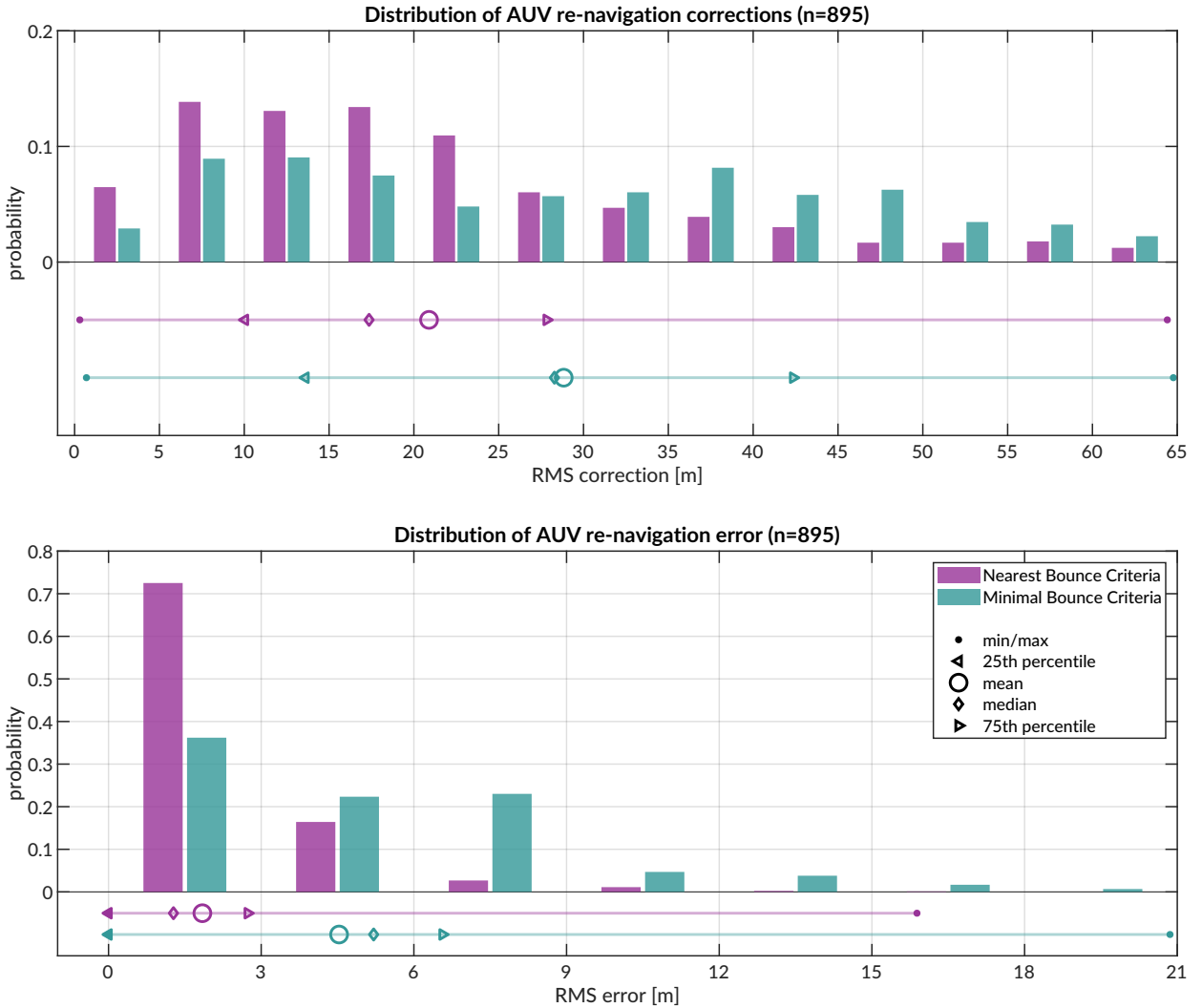


FIG. 12. Distribution of vehicle re-navigation corrections (top) and error (bottom) computed in post-processing for the Minimum and Nearest Bounce Criterion.

501 The top panel shows the connections between the North and East buoys. There is relative, i.e. non-rigid, ice movement between the North and East buoys, evidenced by events spanning the dashed line. But the height of the scatter plot is indicative of the precision of the GPS signal, as it remains consistent across many arrival time bands. Naturally, some minor offsets between these vertical bands relate to different operational configurations of

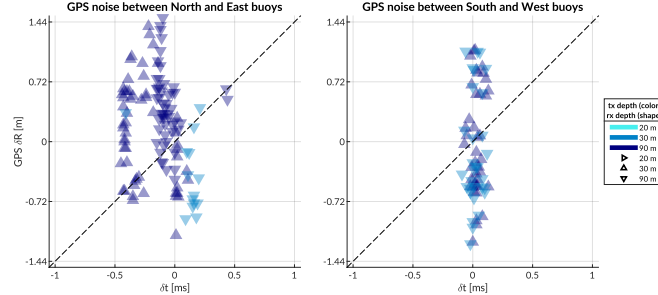


FIG. 13. A comparison of GPS drift (y-axis) versus OWTT drift (x-axis), colored by source and receiver depth. The physical link between North and East are shown on the top; South and West is on the bottom.

506 source and receiver depth. However, the large majority of events show vertical banding for  
 507 the same nominal  $\delta t$ , indicating the amount of GPS drift.

508 This idea of GPS drift relative to the same OWTT measurements is further indicated by  
 509 events between the other two buoys, South and West, in the bottom panel. These buoys are  
 510 moving in a more rigid ice floe and there is minimal impact by source and receiver depth  
 511 on the spread of OWTT. The GPS drift is much larger relative to the OWTT drift, which  
 512 is sensitive to acoustic scattering, multipath, and/or environmental microstructure.

513 These are just two subsets of the physical links that cover all four GPS modem buoys. The  
 514 GPS at camp is the least accurate due to the human activity and infrastructure occluding  
 515 the physical puck.

## 516 VI. DISCUSSION

517 Given the computational constraints of real-time modeling, the gridded approach facil-  
 518 itates enough multipath classification to build in a “ray ensemble” of characteristic group

519 velocities. This result is not always possible when aiming to find eigenrays to just an individual point, even with a higher density of launch angles. An important takeaway for those  
 520 interested in ray-based localization is leveraging a local grid to give BELLHOP tolerance  
 521 for finding solutions that otherwise may not be found in a center or single point solution.  
 522 The limitations of numerical computation, particularly for a complex environment, are more  
 523 adeptly addressed by accepting some uncertainty in position than by prescribing an exact  
 524 solution. Even though BELLHOP is a greedy estimator for eigenrays, the additional data  
 525 created is a negligible burden.

527 Underwater navigation research is broadly motivated by acquiring GPS-like navigation  
 528 accuracy in GPS-denied conditions. The Arctic, while remote, is the perfect place to test  
 529 mature navigation technologies in real GPS-denied conditions.

530 Range estimation is an essential step of acoustic localization and navigation. Current  
 531 approaches in real-time underwater acoustic navigation simplify the non-linear relationship  
 532 between a sound speed profile and acoustic propagation with a deterministic sound speed.  
 533 Some post-processing approaches attempt to leverage the acoustic arrival structure via var-  
 534 ious ray methods, but often use a singular SSP for simplicity, even over long term missions  
 535 or dynamic conditions. Thus, the conversion from travel time to range, particularly for  
 536 real-time vehicle deployments, can be pre-conditioned for error growth as the OWTT/range  
 537 increases.

538 For GPS-denied navigation, especially in hostile environments like the Arctic, tolerance  
 539 for error is close to none. This work addresses a critical need in acoustic navigation by

540 retooling acoustic arrival methods generally deemed too complex or labor intensive for real-  
 541 time, ray-based range estimation to achieve GPS-like positioning.

542 We hypothesize and validate that the embedded stochastic prediction of a single group  
 543 velocity is a smoothly varying function of range, source and receiver depth pairings, as  
 544 well as multipath structure. We employ a GPS-tracked experiment to have a ground truth  
 545 comparison for real-time localization algorithms. The real-time system achieves GPS-like  
 546 navigation for an AUV without taking into account multipath structure; the ranging error  
 547 improves by an order of magnitude with the suggested multipath adaptability, minimizing  
 548 range error to single meters. Post-processing analysis shows that this method of ranging is  
 549 sensitive to GPS drift itself; thus embedding a stochastic prediction of the horizontal group  
 550 velocity has an outsized benefit to minimizing trilateration error.

551 There are many avenues through which this approach can be further refined and tested for  
 552 field operations. Amongst them is defining the uncertainty grid for BELLHOP via stochastic  
 553 or data-driven measures such as the distance traveled by the AUV between ICNN updates  
 554 or the magnitude of the position corrections by the ICNN. Another is to entirely remove the  
 555 seeded range and instead rely on the submerged asset's depth and recorded OWTT to find  
 556 high probability fields in range.

557 The literature in underwater acoustic navigation and positioning is either real-time or  
 558 physics-based. In this paper we demonstrate a field-tested approach that is both real-time  
 559 and physics-based; this is achieved by coupling data streams with fast acoustic modeling.  
 560 The methods exploit the upward refracting nature and the total ice cover of the Arctic  
 561 environment to achieve remarkable ranging accuracy and precision. It transforms multipath,

562 widely considered as an obstacle for acoustic ranging, into a new information content to  
 563 refine ranging accuracy. We believe that this work enables more accurate range estimation,  
 564 localization, and/or navigation for any field experiment given known source and receiver  
 565 depths.

566 Performance in other acoustic environments may require introducing a different thresh-  
 567 olded metric to sort time of arrivals. Given the NBC algorithm's improvement with increased  
 568 multipath, its effectiveness is likely only challenged by the valid operational scales of a range  
 569 independent propagation environment. For mesoscale operations, like that of many glid-  
 570 ers, the group velocity criteria may need to be modified to better account for variability  
 571 driven by range dependent propagation through internal waves, eddies, or even bathymetric  
 572 changes like underwater volcanoes. BELLHOP simulations provide other relevant eigenray  
 573 information, like time and angle of arrival, that is ripe for statistical and machine learning  
 574 methods to classify a representative group velocity. A bespoke and fast ray tracing method,  
 575 which was used during ICEX20 to evaluate the acoustic fit of sound speed profile parame-  
 576 terization ([Bhatt et al., 2022](#)), can easily report back the number of turning points instead  
 577 of the number of bounces for multipath classification.

578 This approach will start to break down in extremely dynamic environments, like fast  
 579 moving fronts. Realistic *in situ* considerations of the acoustic environment may not be pos-  
 580 sible without complete through-the-sensor integration of acoustic dat and/or hyper realistic  
 581 ocean models.

582 Many approaches to underwater navigation combine it with acoustic tomography, i.e.,  
 583 a joint estimation of both source and receiver locations and the ocean volume between

them. There has been considerable success at this effort in post-processing methods, which utilize intensive—and due to the non-linearity of sound propagation, often brute force—computational methods. For vehicle operations, fast tomography is the ideal implementation, in that one can fully consider how sound speed structure, horizontally and vertically, influences sound propagation. AUVs can serve as moving sources to better image the ocean volume (Deffenbaugh, 1997; Elisseeff *et al.*, 2002), where mobile tomography and navigation converge on the same set of component technologies: position estimation, sound speed parameterization estimation, ray path identification, and vehicle path optimization.

But there are overwhelming challenges, operationally and computationally, for fast, mobile tomography to become a realistic endeavor. Addressing the spatial and temporal scales of what can be solved deterministically and what must be solved stochastically imposes a resolution constraint on the utility of gridded models—resolving fine features inaccurately (or with a false sense of confidence) could be more harmful than assuming range independence. Given that AUV operations are often on small spatial and temporal scales, the added benefit of a gridded model is quite small, and in cases like the Arctic, may actually mischaracterize the ocean volume. For gliders, with longer and larger operational scales, an ocean model may provide more useful information. Currently gliders are low power and do not have the storage or computational power to run a full-scale, realistic ocean model. A lightweight representation of the key environmental and acoustic features, passed through the same manner of acoustic message from the modem experiment, may drastically improve glider navigation.

605 **ACKNOWLEDGMENTS**

606 We acknowledge the significant operational effort spearheaded by the LAMSS ICEX20  
 607 team and all our collaborators. Bhatt was funded by a National Defense, Science, and  
 608 Engineering Graduate Fellowship. This work was supported by the Office of Naval Research  
 609 322-OA under ICEX20 (N00014-17-1-2474) and Task Force Ocean (N00014-19-1-2716).

610

611 Ballard, M. S., Badiey, M., Sagers, J. D., Colosi, J. A., Turgut, A., Pecknold, S., Lin, Y.-T.,  
 612 Proshutinsky, A., Krishfield, R., Worcester, P. F., and Dzieciuch, M. A. (**2020**). “Tem-  
 613 poral and spatial dependence of a yearlong record of sound propagation from the Canada  
 614 Basin to the Chukchi Shelf,” The Journal of the Acoustical Society of America **148**(3),  
 615 1663–1680, <http://asa.scitation.org/doi/10.1121/10.0001970http://files/814/>  
 616 [Ballardetal.-2020-Temporalandspatialdependenceofayearlongreco.pdf](#), doi: [10.](https://doi.org/10.1121/10.0001970)  
 617 [1121/10.0001970](https://doi.org/10.1121/10.0001970).

618 Barker, L. D. L., Jakuba, M. V., Bowen, A. D., German, C. R., Maksym, T., Mayer,  
 619 L., Boetius, A., Dutrieux, P., and Whitcomb, L. L. (**2020**). “Scientific challenges and  
 620 present capabilities in underwater robotic vehicle design and navigation for oceanographic  
 621 exploration under-ice,” Remote Sensing **12**(16), 1–31, doi: [10.3390/RS12162588](https://doi.org/10.3390/RS12162588).

622 Bellingham, J., Leonard, J., Vaganay, J., Goudey, C., Atwood, D., Consi, T., Bales, J.,  
 623 Schmidt, H., and Chryssostomidis, C. (**1995**). “Auv operations in the arctic,” in *Sea Ice  
 624 Mechanics and Arctic Modeling Workshop*.

- 625 Bhatt, E. C. (2021). “A Virtual Ocean framework for environmentally adaptive, em-  
 626 bedded acoustic navigation on autonomous underwater vehicles,” Ph.D. thesis, Mas-  
 627 sachusetts Institute of Technology and Woods Hole Oceanographic Institution Joint Pro-  
 628 gram, <https://hdl.handle.net/1912/27309>, doi: [10.1575/1912/27309](https://doi.org/10.1575/1912/27309).
- 629 Bhatt, E. C., Howard, B., and Schmidt, H. (2022). “An Embedded Tactical Decision Aid  
 630 Framework for Environmentally Adaptive Autonomous Underwater Vehicle Communica-  
 631 tion and Navigation,” IEEE Journal of Oceanic Engineering .
- 632 Brooke, J. (1981). “Arcs (autonomous remotely controlled submersible),” in *Proceedings of*  
 633 *the 1981 2nd International Symposium on Unmanned Untethered Submersible Technology*,  
 634 IEEE, Vol. 2, pp. 28–28.
- 635 Chassignet, E. P., Hurlburt, H. E., Smedstad, O. M., Halliwell, G. R., Hogan, P. J., Wall-  
 636 craft, A. J., Baraille, R., and Bleck, R. (2007). “The HYCOM (HYbrid Coordinate  
 637 Ocean Model) data assimilative system,” Journal of Marine Systems **65**(1-4), 60–83, doi:  
 638 [10.1016/J.JMARSYS.2005.09.016](https://doi.org/10.1016/J.JMARSYS.2005.09.016).
- 639 Chen, R., Poulsen, A., and Schmidt, H. (2019). “Spectral, spatial, and tem-  
 640 poral characteristics of underwater ambient noise in the Beaufort Sea in 1994  
 641 and 2016,” The Journal of the Acoustical Society of America **145**(2), 605–  
 642 614, <https://asa.scitation.org/doi/full/10.1121/1.5088601http://files/757/>  
 643 [Chenetal.-2019-Spectral,spatial, and temporal characteristics of.pdf](https://files/757/Chenetal.-2019-Spectral,spatial, and temporal characteristics of.pdf), doi: 10.  
 644 [1121/1.5088601](https://doi.org/10.1121/1.5088601).
- 645 Chen, R., and Schmidt, H. (2020). “Temporal and spatial charac-  
 646 teristics of the Beaufort Sea ambient noise environment,” The Jour-

- 647      nal of the Acoustical Society of America **148**(6), 3928–3941, <https://doi.org/10.1121/10.0002955>
- 648      //asa.scitation.org/doi/full/10.1121/10.0002955http://files/755/
- 649      [ChenandSchmidt-2020-TemporalandspatialcharacteristicsoftheBeaufou.pdf](#), doi:
- 650      [10.1121/10.0002955](https://doi.org/10.1121/10.0002955).
- 651      Claus, B., Kepper, J. H., Suman, S., and Kinsey, J. C. (2018). “Closed-loop one-way-travel-
- 652      time navigation using low-grade odometry for autonomous underwater vehicles,” Journal
- 653      of Field Robotics **35**(4), 421–434, doi: [10.1002/rob.21746](https://doi.org/10.1002/rob.21746).
- 654      Council, N. R. (2011). *National Security Implications of Climate Change for U.S. Naval Forces* (The National Academies Press, Washington, DC), <https://www.nap.edu/catalog/12914/national-security-implications-of-climate-change-for-us-naval-forces>.
- 655      Deffenbaugh, M. (1997). “Optimal Ocean Acoustic Tomography and Navigation with Moving Sources,” Ph.D. thesis, MIT-WHOI Joint Program in Oceanography/Applied Ocean
- 656      Science and Engineering.
- 657      Deffenbaugh, M., Bellingham, J. G., and Schmidt, H. (1996a). “Relationship between
- 658      spherical and hyperbolic positioning,” Oceans Conference Record (IEEE) **2**, 590–595, doi:
- 659      [10.1109/OCEANS.1996.568293](https://doi.org/10.1109/OCEANS.1996.568293).
- 660      Deffenbaugh, M., Schmidt, H., and Bellingham, J. G. (1996b). “Acoustic positioning in a
- 661      fading multipath environment,” in *OCEANS 96 MTS/IEEE Conference Proceedings. The*
- 662      *Coastal Ocean-Prospects for the 21st Century*, IEEE, Vol. 2, pp. 596–600.
- 663      Duda, T. F., Morozov, A. K., Howe, B. M., Brown, M. G., Speer, K., Lazarevich,
- 664      P., Worcester, P. F., and Cornuelle, B. D. (2006). “Evaluation of a long-range joint

- 669 acoustic navigation / thermometry system," in *Oceans 2006*, pp. 1–6, <http://files/939/Dudaetal.-2006-EvaluationofaLong-RangeJointAcousticNavigati.pdf> <http://files/940/4099137.html>, doi: [10.1109/OCEANS.2006.306999](https://doi.org/10.1109/OCEANS.2006.306999).
- 670
- 671
- 672 Duda, T. F., Zhang, W. G., and Lin, Y.-T. (2021). "Effects of Pacific Summer Water layer  
673 variations and ice cover on Beaufort Sea underwater sound ducting," *The Journal of the  
674 Acoustical Society of America* **149**(4), 2117–2136, doi: [10.1121/10.0003929](https://doi.org/10.1121/10.0003929).
- 675 Duda, T. F., Zhang, W. G., Lin, Y.-T., and Newhall, A. E. (2019). "Long-  
676 range sound propagation in the Canada Basin," <http://files/565/Dudaetal.-Unknown-LONG-RANGESOUNDPROPAGATIONINTHECANADABASIN.pdf>.
- 677
- 678 Elisseeff, P., Schmidt, H., and Xu, W. (2002). "Ocean acoustic tomography as a data assimilation problem," *IEEE Journal of Oceanic Engineering* **27**(2), 275–282, <http://files/438/Elisseeff,Schmidt,Xu-2002-OceanAcousticTomographyasaDataAssimilationProblem.pdf>, doi: [10.1109/JOE.2002.1002482](https://doi.org/10.1109/JOE.2002.1002482).
- 681
- 682
- 683 Eustice, R. M., Whitcomb, L. L., Singh, H., and Grand, M. (2006). "Recent advances in  
684 synchronous-clock one-way-travel-time acoustic navigation," *Oceans 2006* doi: [10.1109/OCEANS.2006.306931](https://doi.org/10.1109/OCEANS.2006.306931).
- 685
- 686 Eustice, R. M., Whitcomb, L. L., Singh, H., and Grund, M. (2007). "Experimental results in synchronous-clock one-way-travel-time acoustic navigation for autonomous underwater vehicles," in *Proceedings - IEEE International Conference on Robotics and Automation*, pp. 4257–4264, <http://files/877/Eusticeetal.-2007-ExperimentalResultsinSynchronous-ClockOne-Way-.pdf> <http://files/877/Eusticeetal.-2007-ExperimentalResultsinSynchronous-ClockOne-Way-.pdf>
- 689
- 690

- 691    <http://files/878/4209752.html>, doi: [10.1109/ROBOT.2007.364134](https://doi.org/10.1109/ROBOT.2007.364134).
- 692    Fossum, T. O., Norgren, P., Fer, I., Nilsen, F., Koenig, Z. C., and Ludvigsen, M. (2021).
- 693    “Adaptive sampling of surface fronts in the arctic using an autonomous underwater ve-
- 694    hicle,” IEEE Journal of Oceanic Engineering **46**(4), 1155–1164, doi: [10.1109/JOE.2021.3070912](https://doi.org/10.1109/JOE.2021.3070912).
- 695
- 696    Freitag, L., Ball, K., Partan, J., Koski, P., and Singh, S. (2016). “Long range acoustic
- 697    communications and navigation in the Arctic,” OCEANS 2015 - MTS/IEEE Washington
- 698    2–6, doi: [10.23919/oceans.2015.7401956](https://doi.org/10.23919/oceans.2015.7401956).
- 699    Graupe, C. E., Van Uffelen, L. J., Webster, S. E., Worcester, P. F., and Dzieci-
- 700    uch, M. A. (2019). “Preliminary results for glider localization in the Beau-
- 701    fort Duct using broadband acoustic sources at long range,” in *OCEANS 2019*
- 702    *MTS/IEEE Seattle, OCEANS 2019*, pp. 1–6, <http://files/763/Graupeetal.-2019-Preliminaryresultsforgliderlocalizationinthe.pdf>
- 703
- 704    <http://files/764/8962637.html> <http://files/913/8962637.html>, doi: [10.23919/OCEANS40490.2019.8962637](https://doi.org/10.23919/OCEANS40490.2019.8962637).
- 705
- 706
- 707    Hayes, D. R., and Morison, J. H. (2002). “Determining turbulent vertical velocity, and
- 708    fluxes of heat and salt with an autonomous underwater vehicle,” Journal of Atmospheric
- 709    and Oceanic Technology **19**(5), 759–779.
- 710    Howe, B. M., Miksis-Olds, J., Rehm, E., Sagen, H., Worcester, P. F., and Haral-
- 711    abus, G. (2019). “Observing the Oceans Acoustically,” Frontiers in Marine Science **6**,
- 712    426, <https://www.frontiersin.org/article/10.3389/fmars.2019.00426/full>, doi:

713 10.3389/fmars.2019.00426.

714 Jackson, E. (1983). “Autonomous remotely controlled submersible “ARCS”,” in *Proceedings*  
 715 of the 1983 3rd International Symposium on Unmanned Untethered Submersible Technol-  
 716 ogy, IEEE, Vol. 3, pp. 77–88.

717 Jakuba, M. V., Roman, C. N., Singh, H., Murphy, C., Kunz, C., Willis, C., Sato,  
 718 T., and Sohn, R. A. (2008). “Long-baseline acoustic navigation for under-ice  
 719 autonomous underwater vehicle operations,” *Journal of Field Robotics* **25**(11-12),  
 720 861–879, <https://onlinelibrary.wiley.com/doi/full/10.1002/rob.20250>  
 721 <https://onlinelibrary.wiley.com/doi/abs/10.1002/rob.20250>  
 722 <https://onlinelibrary.wiley.com/doi/10.1002/rob.20250>, doi: 10.1002/ROB.20250.

723 Kepper, J. H., Claus, B. C., and Kinsey, J. C. (2017). “MEMS IMU and one-  
 724 way-travel-time navigation for autonomous underwater vehicles,” in *OCEANS*  
 725 2017 - Aberdeen, Vol. 2017-Octob, pp. 1–9, <http://files/550/Kepper,Claus,Kinsey-2017-MEMSIMUandOne-Way-Travel-TimeNavigationforAutonomousUnderwaterVehicles.pdf>,  
 726 doi: 10.1109/OCEANSE.2017.8084842.

728 Krishfield, R., Toole, J., Proshutinsky, A., and Timmermans, M. L. (2008). “Automated  
 729 ice-tethered profilers for seawater observations under pack ice in all seasons,” *Journal of*  
 730 *Atmospheric and Oceanic Technology* **25**(11), 2091–2105, doi: 10.1175/2008JTECH0587.

731 1.

732 Kukulya, A., Plueddemann, A., Austin, T., Stokey, R., Purcell, M., Allen, B., Littlefield, R.,  
 733 Freitag, L., Koski, P., Gallimore, E. et al. (2010). “Under-ice operations with a remus-100  
 734 auv in the arctic,” in *2010 IEEE/OES Autonomous Underwater Vehicles*, IEEE, pp. 1–8.

- 735 Kunz, C., Murphy, C., Camilli, R., Singh, H., Bailey, J., Eustice, R., Jakuba, M., Nakamura,  
 736 K., Roman, C., Sato, T., Sohn, R., and Willis, C. (2008). “Deep sea underwater robotic  
 737 exploration in the ice-covered Arctic ocean with AUVs,” in *2008 IEEE/RSJ International*  
 738 *Conference on Intelligent Robots and Systems*, IEEE, pp. 3654–3660, <http://files/875/Kunzetal.-2008-Deepseaunderwaterroboticexplorationintheice.pdf>  
 739 <http://files/968/Kunzetal.-2008-Deepseaunderwaterroboticexplorationintheice.pdf>  
 740 <http://ieeexplore.ieee.org/document/4651097/>, doi: [10.1109/IROS.2008.4651097](https://doi.org/10.1109/IROS.2008.4651097).
- 742 Light, R., and Morison, J. (1989). “The autonomous conductivity-temperture vehicle: First  
 743 in the seashuttle family of autonomous underwater vehicle’s for scientific payloads,” in  
 744 *Proceedings OCEANS*, Vol. 3, pp. 793–798, doi: [10.1109/OCEANS.1989.586683](https://doi.org/10.1109/OCEANS.1989.586683).
- 746 Litvak, A. (2015). “Acoustics of the deepwater part of the arctic ocean and of russia’s  
 747 arctic shelf,” *Herald of the Russian Academy of Sciences* **85**, 239–250, doi: [10.1134/S1019331615030144](https://doi.org/10.1134/S1019331615030144).
- 749 Mikhalevsky, P. N., Sperry, B. J., Woolfe, K. F., Dzieciuch, M. A., and Worces-  
 750 ter, P. F. (2020). “Deep ocean long range underwater navigation,” *The Jour-*  
 751 *nal of the Acoustical Society of America* **147**(4), 2365–2382, <http://asa.scitation.org/doi/10.1121/10.0001081>  
 752 <http://files/631/Mikhalevskyetal.-2020-Deepeceanlongrangeunderwaternavigation.pdf>, doi: [10.1121/10.0001081](https://doi.org/10.1121/10.0001081).
- 754 Norgren, P., Lubbad, R., and Skjetne, R. (2014). “Unmanned underwater vehicles in Arctic  
 755 operations,” in *22nd IAHR International Symposium on Ice*.

- 756 Paull, L., Saeedi, S., Seto, M., and Li, H. (2014). *AUV navigation and*  
 757 *localization: A review*, **39**, pp. 131–149, <http://files/127/Paulletal.-2014-AUVnavigationandlocalizationAreview.pdf>.
- 759 Plueddemann, A. J., Kukulya, A. L., Stokey, R., and Freitag, L. (2012). “Autonomous  
 760 Underwater Vehicle Operations Beneath Coastal Sea Ice,” IEEE/ASME Transactions  
 761 on Mechatronics **17**(1), 54–64, doi: [10.1109/TMECH.2011.2174798](https://doi.org/10.1109/TMECH.2011.2174798) conference Name:  
 762 IEEE/ASME Transactions on Mechatronics.
- 763 Porter, M. B. (2011). “The BELLHOP Manual and User’s Guide,” HLS Research, , 2010  
 764 1–57, <http://oalib.hlsresearch.com/Rays/HLS-2010-1.pdf>.
- 765 Poulsen, A. J., and Schmidt, H. (2017). “Acoustic noise properties in the rapidly changing  
 766 Arctic Ocean,” **070005**(2016), 070005, doi: [10.1121/2.0000552](https://doi.org/10.1121/2.0000552).
- 767 Randeni, S., Schneider, T., and Schmidt, H. (2020). “Construction of a  
 768 high-resolution under-ice AUV navigation framework using a multidisci-  
 769 plinary virtual environment,” in *2020 IEEE/OES Autonomous Underwater  
 770 Vehicles Symposium, AUV 2020*, pp. 1–7, <http://files/689/Randenietal.-2020-Constructionofahigh-resolutionunder-iceAUVna.pdf>, doi: [10.1109/AUV50043.2020.9267950](https://doi.org/10.1109/AUV50043.2020.9267950).
- 771
- 772
- 773 Randeni, S., Schneider, T., Schmidt, H., Bhatt, E., and Viquez, O. (2021). “A high-  
 774 resolution AUV navigation framework with integrated communication and tracking for  
 775 under-ice deployments,” *Field Robotics* (in review).
- 776 Rossby, T., Dorson, D., and Fontaine, J. (1986). “The RAFOS System,” *Journal of Atmo-*  
 777 *spheric and Oceanic Technology* **3**, 148–162.

- 778 Rypkema, N. R., Fischell, E. M., and Schmidt, H. (2017). “One-Way Travel-Time Inverted  
 779 Ultra-Short Baseline Localization for Low-Cost Autonomous Underwater Vehicles,” in *2017*  
 780 *IEEE International Conference on Robotics and Automation (ICRA)*, Singapore, pp. 4920–  
 781 4926.
- 782 Schmidt, H., and Schneider, T. (2016). “Acoustic communication and navigation in  
 783 the new Arctic-A model case for environmental adaptation,” 3rd Underwater Com-  
 784 munications and Networking Conference, Ucomms 2016 <http://files/583/Schmidt,Schneider-2016-AcousticCommunicationandNavigationintheNewArctic-AModelCaseforEnvironment.pdf>, doi: [10.1109/UComms.2016.7583469](https://doi.org/10.1109/UComms.2016.7583469).
- 787 Schneider, T., and Schmidt, H. (2018). “NETSIM: A realtime virtual ocean hardware-  
 788 in-the-loop acoustic modem network simulator,” in *2018 4th Underwater Communi-*  
 789 *cations and Networking Conference, UComms 2018*, pp. 1–5, <http://files/1047/SchneiderandSchmidt-2018-NETSIMARealtimeVirtualOceanHardware-in-the-l.pdf>, doi: [10.1109/UComms.2018.8493188](https://doi.org/10.1109/UComms.2018.8493188).
- 792 Schneider, T., Schmidt, H., and Randeni, S. (2020). “Self-Adapting Under-Ice Inte-  
 793 grated Communications and Navigation Network,” 2020 5th Underwater Communica-  
 794 tions and Networking Conference, UComms 2020 5, <http://files/607/Schneideretal.-Self-AdaptingUnder-IceIntegratedCommunications.pdf>.
- 796 Singh, S., Grand, M., Bingham, B., Eustice, R., Singh, H., and Freitag, L. (2006).  
 797 “Underwater acoustic navigation with the WHOI Micro-Modem,” in *Oceans 2006*,  
 798 IEEE, pp. 1–4, <http://ieeexplore.ieee.org/document/4099008/> <http://files/774/Singhetal.-2006-UnderwaterAcousticNavigationwiththeWHOIMicro.pdf>, doi: [10.1109/OCEANS.2006.1700001](https://doi.org/10.1109/OCEANS.2006.1700001).

800 1109/OCEANS.2006.306853.

801 Timmermans, M.-L., and Winsor, P. (2013). “Scales of horizontal density structure in the  
802 chukchi sea surface layer,” Continental Shelf Research **52**, 39–45.

803 Toole, J. M., Krishfield, R. A., Timmermans, M. L., and Proshutinsky, A. (2011). “The  
804 Ice-Tethered profiler: Argo of the Arctic,” Oceanography **24**(3), 126–135, doi: [10.5670/oceanog.2011.64](https://doi.org/10.5670/oceanog.2011.64).

805 Uffelen, L. J. V., Howe, B. M., Nosal, E.-M., Carter, G. S., Worcester, P. F., and Dzieciuch,  
806 M. A. (2016). “Localization and subsurface position error estimation of gliders using  
807 broadband acoustic signals at long range,” IEEE Journal of Oceanic Engineering **41**(3),  
808 501–508.

809 Van Uffelen, L. J. (2021). “Global Positioning Systems: Over Land and Under Sea,” Acoustics  
810 Today **17**(1), 52, doi: [10.1121/at.2021.17.1.52](https://doi.org/10.1121/at.2021.17.1.52).

811 Van Uffelen, L. J., Nosal, E.-M., Howe, B. M., Carter, G. S., Worcester, P. F., Dzieciuch,  
812 M. A., Heaney, K. D., Campbell, R. L., and Cross, P. S. (2013). “Estimating uncertainty  
813 in subsurface glider position using transmissions from fixed acoustic tomography sources,”  
814 The Journal of the Acoustical Society of America **134**(4), 3260–3271, doi: [10.1121/1.4818841](https://doi.org/10.1121/1.4818841).

815 Webster, S. E., Eustice, R. M., Singh, H., and Whitcomb, L. L. (2009). “Preliminary  
816 deep water results in single-beacon one-way-travel-time acoustic navigation  
817 for underwater vehicles,” 2009 IEEE/RSJ International Conference on Intelligent  
818 Robots and Systems, IROS 2009 2053–2060, <http://files/416/Websteretal.-2009-Preliminarydeepwaterresultsinsingle-beaconone-way-travel-timeacousticnavigationf>

- 822 pdf, doi: [10.1109/IROS.2009.5354457](https://doi.org/10.1109/IROS.2009.5354457).
- 823 Webster, S. E., Eustice, R. M., Singh, H., and Whitcomb, L. L. (2012). “Advances in  
824 single-beacon one-way-travel-time acoustic navigation for underwater vehicles,” Interna-  
825 tional Journal of Robotics Research **31**(8), 935–950, doi: [10.1177/0278364912446166](https://doi.org/10.1177/0278364912446166).
- 826 Webster, S. E., Freitag, L. E., Lee, C. M., and Gobat, J. I. (2015). “Towards real-time  
827 under-ice acoustic navigation at mesoscale ranges,” in *Proceedings - IEEE International  
828 Conference on Robotics and Automation*, June, IEEE, pp. 537–544, [http://files/625/  
829 Websteretal.-2015-Towardsreal-timeunder-iceacousticnavigationat.pdf](http://files/625/Websteretal.-2015-Towardsreal-timeunder-iceacousticnavigationat.pdf) <http://files/641/Websteretal.-2015-Towardsreal-timeunder-iceacousticnavigationat.pdf>
- 830 <http://files/835/Websteretal.-2015-Towardsreal-timeunde>, doi: [10.1109/ICRA.2015.7139231](https://doi.org/10.1109/ICRA.2015.7139231).
- 831 Wu, M., Barmin, M. P., Andrew, R. K., Weichman, P. B., White, A. W., Lavely, E. M.,  
832 Dzieciuch, M. A., Mercer, J. A., Worcester, P. F., and Ritzwoller, M. H. (2019).  
833 “Deep water acoustic range estimation based on an ocean general circulation model:  
834 Application to PhilSea10 data,” The Journal of the Acoustical Society of America  
835 **146**(6), 4754–4773, <https://doi.org/10.1121/1.5138606> <http://files/947/Wuetal.-2019-Deepwateracousticrangeestimationbasedonano.pdf>
- 836 <http://files/948/1.html>, doi: [10.1121/1.5138606](https://doi.org/10.1121/1.5138606).
- 837
- 838
- 839